Minoo Afshar
Wolfgang Thormann

Department of Clinical Pharmacology,
University of Bern,
Bern, Switzerland

Received September 7, 2005
Revised December 6, 2005
Accepted December 6, 2005

Research Article

Capillary electrophoretic investigation of the enantioselective metabolism of propafenone by human cytochrome P-450 SUPERSOMES: Evidence for atypical kinetics by CYP2D6 and CYP3A4

An enantioselective CE method was used to identify the ability of CYP450 enzymes and their stereoselectivity in catalyzing the transformation of propafenone (PPF) to 5-hydroxy-propafenone (5OH-PPF) and *N*-despropyl-propafenone (NOR-PPF). Using *in vitro* incubations with single CYP450 enzymes (SUPERSOMES), 5OH-PPF is shown to be selectively produced by CYP2D6 and *N*-dealkylation is demonstrated to be mediated by CYP2D6, CYP3A4, CYP1A2, and CYP1A1. For the elucidation of kinetic aspects of the metabolism with CYP2D6 and CYP3A4, incubations with individual PPF enantiomers and racemic PPF were investigated. With the exception of the dealkylation in presence of *R*-PPF only, which can be described by the Michaelis–Menten model, all CYP2D6-induced reactions were found to follow autoactivation kinetics. For CYP3A4, all NOR-PPF enantiomer formation rates as function of PPF enantiomer concentration were determined to follow substrate inhibition kinetics. The formation of NOR-PPF by the different enzymes is stereoselective and is reduced significantly when racemic PPF is incubated. Clearance values obtained for CYP3A4 dealkylation are stereoselective whereas those of CYP2D6 hydroxylation are not. This paper reports the first investigation of the PPF hydroxylation and dealkylation kinetics by the CYP2D6 enzyme and represents the first report in which enantioselective CE data provide the complete *in vitro* kinetics of metabolic steps of a drug.

Keywords: 5-Hydroxy-propafenone / *in vitro* metabolism / *N*-Despropyl-propafenone / Stereoselective metabolism / Sulfated β-cyclodextrin DOI 10.1002/elps.200500664

1 Introduction

Cytochrome P450 enzymes (CYPs) are the dominant enzyme systems that control drug metabolism and clearance [1]. These enzymes are particularly prominent in hepatic tissue, where they catalyze the NADPH-dependent mono-oxygenation of structurally diverse lipophilic substrates to yield more polar derivatives [2]. As drug biotransformation is a determinant of drug pharmacokinetics, therapeutic efficacy, and toxic effects, the elucidation of metabolic routes, metabolizing enzymes and their kinetics, and metabolic interactions are important for all marketed drugs. This is the rationale for the use of *in vivo* and *in vitro* methods to assess drug metabolism and metabolic interactions.

Propafenone (PPF, for chemical structure see Fig. 1) is an antiarrhythmic agent with fast sodium channel-blocking activity, which has been proven to be effective in the control of supraventricular and ventricular arryhthmias. PPF also has some β-blocking action, much less than that of propranolol, and has a weak calcium channel-blocking effect [3, 4]. PPF is a chiral compound which is administered as a racemic mixture. Although equipotent in the sodium channel-blocking activity, *S*-PPF is almost 100 times more potent at β-adrenergic receptors than *R*-PPF. In humans, PPF undergoes extensive metabolism

Correspondence: Professor Dr. Wolfgang Thormann, Department of Clinical Pharmacology, Murtenstrasse 35, CH-3010 Bern, Switzerland
E-mail: wolfgang.thormann@ikp.unibe.ch
Fax: +41-31-632-4997

Abbreviations: CYP, cytochrome P450 enzyme; **HLM**, human liver microsomes; **IS**, internal standard; **NOR-PPF**, *N*-despropyl-propafenone; **5OH-PPF**, 5-hydroxy-propafenone; **PPF**, propafenone

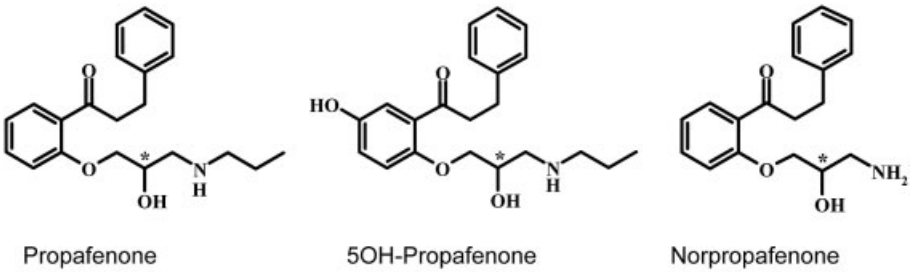

Figure 1. Chemical structures of PPF, 5OH-PPF, and norpropafenone.

(approximately 100% of the dose), with 5-hydroxy-propafenone (5OH-PPF, Fig. 1) and *N*-despropyl-propafenone (NOR-PPF, Fig. 1) being the major active metabolites. It has been shown that PPF ring hydroxylation is under genetic control and cosegregates with the debrisoquine metabolic phenotype. After oral administration of PPF, *R*-PPF has been shown to have a higher clearance than its antipode, suggesting that PPF is metabolized stereoselectively *in vivo* [5, 6]. Given the stereoselective pharmacodynamic and disposition characteristics of PPF and its specific biotransformation, identification of human CYP isoforms involved in its metabolism and investigation of their enantioselective kinetic profiles has attracted considerable interest. Using human liver microsomes (HLM) together with chemical inhibitors, specific antibodies, and correlation studies, Kroemer *et al.* [7, 8] showed that CYP2D6 catalyzes the 5-hydroxylation whereas CYP3A4 and CYP1A2 mediate the *N*-dealkylation of PPF.

Recently, molecular biology techniques have led to the successful cloning and expression of a large number of human CYP isozymes. Insect cells lack endogenous cytochrome P450 activity and, therefore, microsomes, which consist of vesicles of the hepatocyte endoplasmic reticulum of human CYP-transfected insect cells (SUPERSOMES), can be a useful tool in human biotransformation studies. The availability of specifically expressed human CYPs in SUPERSOMES allows the investigation of the contribution of a single metabolic enzyme to the biotransformation pathway of the compound under investigation [9]. Although the metabolism of PPF has been studied thoroughly in media containing liver microsomes from animals [10–12] and humans [7, 8, 13–15], and in preparations of cryopreserved human and animal hepatocytes [16], the role of individual human CYPs in the metabolism of PPF and their stereoselectivity has not been completely defined. Zhou *et al.* [17, 18] investigated the stereoselective kinetics of PPF in S9 prepared from transgenic Chinese hamster CHL cell lines expressing CYP3A4 and CYP1A2 using a substrate depletion approach, and Botsch *et al.* [8] studied *N*-dealkylation of PPF with microsomal fractions of yeast cells that were genetically engineered for stable expression of CYP1A1, CYP1A2, and CYP3A4. In the latter approach, enantioselectivity of the single enzymes was not investigated. Recent studies in our laboratory with SUPERSOMES have shown that CYP2D6 is involved in the production of NOR-PPF but the kinetics of its formation and its contribution to the NOR-PPF formation remained to be established. In that work, an enantioselective CE method was developed and shown to be suitable for quantitation of the enantiomers of PPF, 5OH-PPF, and NOR-PPF in incubation media containing SUPERSOMES and HLM [19]. Using this CE assay, the *in vitro* work with PPF and SUPERSOMES was continued. The present study had two major goals. One was to screen the human CYPs for their ability to produce 5OH-PPF and NOR-PPF *in vitro*. The other goal was to establish the kinetics and stereoselectivity of the PPF metabolism in media containing human CYP2D6 and CYP3A4 SUPERSOMES.

2 Materials and methods

2.1 Chemicals and reagents

Racemic PPF, *S*-PPF and *R*-PPF (all as hydrochlorides) were obtained from Knoll (Ludwigshafen, Germany). Racemic 5OH-PPF hydrochloride and racemic NOR-PPF fumarate were kindly donated by Dr. Ute Hofmann (Dr. Margarete Fischer-Bosch-Institut für Klinische Pharmakologie, Stuttgart, Germany). Methanol (HPLC-grade), sodium dihydrogen phosphate, orthophosphoric acid, dichloromethane (HPLC-grade), and sodium carbonate were purchased from Merck (Darmstadt, Germany). Sulfated β-CD sodium salt was obtained from Sigma-Aldrich (Schnelldorf, Germany). Double-distilled water was used throughout the study. Atenolol (used as internal standard (IS)) was obtained from the Inselspital Pharmacy (Bern, Switzerland). Microsomes from baculovirus-infected cells expressing CYP1A1, CYP1A2, CYP2C9*1, CYP2C19, CYP2D6*1, and CYP3A4 (SUPERSOMES) were obtained from Gentest (Woburn, MA, USA). All SUPERSOMES were coexpressed with human P450 reductase. CYP2C19, CYP2C9*1, and CYP3A4 were additionally

coexpressed with the human cytochrome b_5. NADPH regenerating systems A and B were also from Gentest. Microsomes were stored at −80°C and were thawed on ice before use. NADPH regenerating system solutions A and B were kept at −20°C.

2.2 Microsomal incubations

Incubation mixtures (500 μL containing 25 μL of solution A and 5 μL of solution B) comprised substrate (racemic PPF, *S*-PPF or *R*-PPF), 1.3 mM $NADP^+$, 3.3 mM glucose-6-phosphate, 0.1 M potassium phosphate buffer (pH 7.5), and methanol (<0.5%, originating from substrate solution). Phosphate buffer (50 mM, pH 7.4) and 100 mM Tris buffer (pH 7.5) instead of the 100 mM pH 7.4 phosphate solution were used for the incubations with CYP2C19 and CYP2C9*1, respectively. The mixtures were first pre-incubated for 10 min at 37°C using an Eppendorf Thermomixer followed by addition of ice-cold SUPERSOMES (12.5 or 25 pmol for kinetic and screening data, respectively) and incubation for 30 min (kinetic data) or 3 h (screening data) at 37°C without shaking. The reactions were terminated on ice and samples were immediately pretreated for CE analysis as described in detail elsewhere [19]. For enzyme kinetics studies, six to nine different enantiomer concentrations in the ranges of 0.8–50 μM (CYP2D6) and 5–1000 μM (CYP3A4) were incubated. Each experiment was carried out in duplicate. Screening data were generated with 50 μM substrate concentrations.

2.3 CE assay

All enantiomer determinations were performed using the method of Afshar and Thormann which is based upon liquid/liquid extraction at alkaline pH followed by CE analysis of the reconstituted extracts [19]. Briefly, a Bio-Focus 3000 instrument (BioRad Laboratories, Hercules, CA, USA) with a 50 μm id fused-silica capillary of 36 cm total length (31.4 cm effective length) and an on-column UV variable wavelength detector set to 195 nm were used. The applied voltage was 13 kV, and the carousels and capillary temperatures were controlled at 25 and 20°C, respectively. The buffer was composed of 100 mM sodium phosphate solution, pH 2.0, 19% methanol, and 0.6% sulfated β-CD. The samples were hydrodynamically injected for 9 psi × s, and the assay was calibrated for each enantiomer between 25 and 1000 ng/mL. Overall accuracy and precision assessed with quality control samples were <15%, and the LOQ for all enantiomers was 25 ng/mL. Experiments were carried out in duplicate, and the mean values were used for data analysis. All metabolite formation rates were expressed as picomol of enantiomer formed *per* hour *per* picomol of CYP.

2.4 Kinetic analysis and calculation of clearance

The kinetic studies were performed with CYP2D6*1 and CYP3A4 SUPERSOMES. The data were fit to the single-site Michaelis–Menten (hyperbolic substrate concentration dependence), autoactivitation (sigmoidal substrate concentration dependence), and substrate inhibition models and further analyzed using Eadie–Hofstee plots [20–23]. The single-site Michaelis–Menten model is based on

$$v = V_{max}[S]/(K_m + [S]) \quad (1)$$

the autoactivation model is expressed by the Hill equation

$$v = V_{max} \cdot [S]^n/(k' + [S]^n) \quad (2)$$

and the substrate inhibition model uses

$$v = V_{max} \cdot [S]/(K_m + [S] + ([S]^2/K_i)) \quad (3)$$

where v is the formation rate (velocity) of the metabolic reaction, [S] is the substrate concentration, K_m is the Michaelis–Menten constant which is the concentration at which the rate of the metabolism is 50% of V_{max}, V_{max} is the maximum formation rate, k' is a constant of the autoactivation model which is equivalent to K_m when $n = 1$, n is the Hill coefficient, and K_i is the substrate inhibition constant. Eadie–Hofstee plots are based on a graphical representation of v *versus* v/[S] and are linear for the Michaelis–Menten model. A deviation from linearity indicates atypical kinetics, including autoactivation or substrate inhibition [22]. Standard parameters such as regression coefficient (R^2), F-test, standard error of the parameter estimates, and visual inspection of Eadie–Hoftsee plots were used to determine the quality of a fit to a specific model. All fits and the determination of the apparent enzyme kinetic parameters, K_m, V_{max}, k', n, and K_i were calculated by nonlinear regression analysis using GraphPad Prism version 4.0 (GraphPad Software, San Diego, CA, USA). For model comparison with the F-test, $p < 0.05$ means that the alternative (non-Michaelis–Menten) model fits the data significantly better.

Intrinsic clearance (CL_{int}), which defines the rate of metabolism for a given drug concentration, and maximal clearance due to autoactivation (CL_{max}), which provides an estimate of the highest clearance attained as substrate concentration increases before any saturation of the enzyme sites were calculated according to [22]

$$CL_{int} = V_{max}/K_m \quad (4)$$

$$CL_{max} = V_{max}/k'[(n-1)/n(n-1)^{1/n}] \quad (5)$$

3 Results

3.1 PPF hydroxylation and *N*-dealkylation with cDNA-expressed human CYPs

The screening of the SUPERSOMES for PPF hydroxylation and *N*-dealkylation was performed with a 3 h incubation of 100 μM racemic PPF and 25 pmol of each enzyme. The data obtained indicated specific and nonspecific catalysis of PPF metabolism, respectively. While 5OH-PPF was formed by CYP2D6 only, NOR-PPF was found to be produced by the CYP1A1, CYP1A2, CYP3A4, and CYP2D6 pathways (Fig. 2). No apparent stereoselectivity was observed for the data obtained with CYP1A2, CYP3A4, and CYP2D6 whereas CYP1A1 was determined to produce NOR-PPF stereoselectively. Under the conditions used to generate the data presented in Fig. 2, the *R*-NOR-PPF/*S*-NOR-PPF concentration ratio was determined to be 1.45. Similar data were observed for 30 min incubations and 12.5 pmol CYP1A1 having 10 μM racemic PPF (*R/S* ratio: 1.38) and 100 μM racemic PPF (*R/S* ratio: 1.55). As CYP1A1 is hardly detected in the liver, no further experiments were performed with this enzyme. CYP2A6, CYP2B6, CYP2C9, and CYP2C19 did not produce any detectable 5OH-PPF and NOR-PPF.

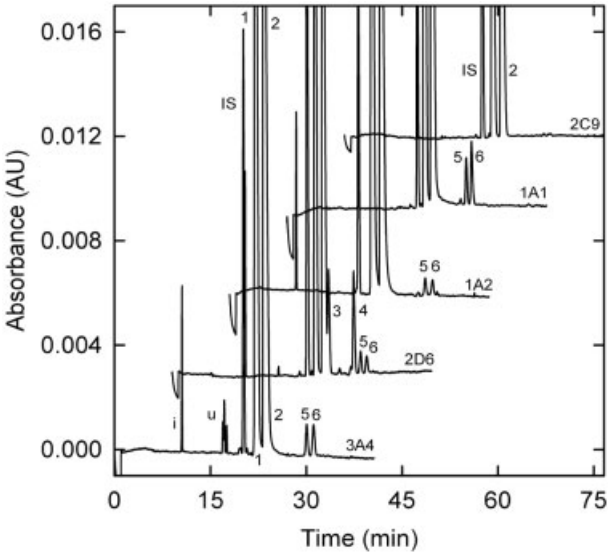

Figure 2. Electropherograms obtained with extracts prepared from 3 h incubations with 100 μM racemic PPF and 25 pmol CYP3A4, CYP2D6, CYP1A2, CYP1A1, and CYP2C9 (from bottom to top, respectively, graphs presented with *x*-axis and *y*-axis scale offsets of 9 min and 0.003 AU, respectively). Hundred micrograms *per* milliliter IS solution was used. Key: 1, *S*-PPF; 2, *R*-PPF; 3, *S*-5OH-PPF; 4, *R*-5OH-PPF; 5, *S*-NOR-PPF; 6, *R*-NOR-PPF; u, unidentified metabolites produced by CYP3A4; and i, peak unrelated to PPF.

The ability of the cDNA-expressed human CYPs to form NOR-PPF with a 30 min incubation at a clinically relevant concentration (10 μM of each enantiomer [24, 25]) and having 12.5 pmol CYP enzyme is further shown with the formation rate data presented in Table 1. The preference of each pathway for catalyzing PPF dealkylation in presence of racemic PPF and of individual PPF enantiomers is thereby documented. For the production of *R*-NOR-PPF, the order of activities is CYP2D6 ≈ CYP3A4>CYP1A2 and CYP1A2>CYP2D6>CYP3A4, respectively. For *S*-PPF, the data reveal the relationships CYP2D6>CYP1A2>CYP3A4 and CYP2D6>CYP3A4>CYP1A2, respectively. For incubation with the racemate, the rates of *S*-NOR-PPF formation became reduced by 48.68, 42.02, and 26.17% in the presence of CYP3A4, CYP2D6, and CYP1A2, respectively. Although the formation rates of *R*-NOR-PPF for the case of CYP3A4 were found to be almost the same in presence of *R*-PPF and the racemate, the rates for the cases with CYP2D6 and CYP1A2 were found to be lower when the racemate was incubated, namely, 36.78 and 61.06%, respectively.

Table 1 also shows an estimate of the contribution of CYP isoforms to PPF *N*-dealkylation in liver microsomes on the basis of the rate of the reaction observed with SUPERSOMES. The preference of CYP isoforms for producing NOR-PPF considering the contribution of an isoform to the total CYP content in the liver [26, 27] was found to be CYP3A4>CYP1A2>CYP2D6. This relationship holds for incubations with racemic PPF and individual PPF enantiomers. As CYP2D6 and CYP3A4 showed the highest contribution to PPF 5-hydroxylation and *N*-dealkylation, respectively, the stereoselective kinetics of PPF hydroxylation and dealkylation in media containing CYP2D6 and CYP3A4 SUPERSOMES was further investigated to gain more clues about the stereoselective clearance of PPF ,which has been reported *in vivo* [5, 6]. To accurately determine kinetic parameters, substrate consumption at all concentrations of substrates was controlled to be less than 15%, and production of metabolites used for quantification of formation rates was linear with incubation time and protein concentration. Furthermore, protein concentration was much smaller than the substrate concentration.

3.2 Kinetics of CYP2D6 mediated hydroxylation and *N*-dealkylation of PPF

The kinetics of PPF hydroxylation and *N*-dealkylation in presence of CYP2D6*1 at the substrate concentration range of 0.8–50 μM for each enantiomer together with corresponding Eadie–Hofstee (*v vs. v*/[S]) plots are shown in Figs. 3, 4, respectively. Computer-derived kinetic parameters for the formation of 5OH-PPF and NOR-PPF

Table 1. Metabolite formation rates and estimation of the contribution of CYP isoforms to PPF *N*-dealkylation in liver microsomes[a)]

Substrate	Enzyme	Metabolite formation rate ($pmol \cdot h^{-1}$ $pmol^{-1}$ CYP)		Relative contribution of isoforms to the total CYP content in liver microsomes[b)]	Predicted metabolite formation rate in liver microsomes[c)] ($pmol \cdot h^{-1}$ $pmol^{-1}$ CYP)		Relative contribution of isoforms to PPF *N*-dealkylation in liver microsomes[d)] (%)	
		R	*S*		*R*	*S*	*R*	*S*
Rac. PPF	CYP1A2	14.89	19.17	0.127	1.89	2.43	21.69	32.75
	CYP2D6	20.90	25.42	0.015	0.31	0.38	3.55	5.12
	CYP3A4	22.60	16.00	0.288	6.51	4.61	74.74	62.13
	CYP2A6	–	–	0.040	–	–	–	–
	CYP2B6	–	–	0.002	–	–	–	–
	CYP2C9	–	–	0.156	–	–	–	–
	CYP2C19	–	–	0.026	–	–	–	–
R – PPF	CYP1A2	38.24	–	0.127	4.86	–	40.29	–
	CYP2D6	33.06	–	0.015	0.49	–	4.06	–
	CYP3A4	23.29	–	0.288	6.71	–	55.64	–
	CYP2A6	–	–	0.040	–	–	–	–
	CYP2B6	–	–	0.002	–	–	–	–
	CYP2C9	–	–	0.156	–	–	–	–
	CYP2C19	–	–	0.026	–	–	–	–
S – PPF	CYP1A2	–	25.96	0.127	–	3.29	–	25.44
	CYP2D6	–	43.84	0.015	–	0.66	–	5.10
	CYP3A4	–	31.17	0.288	–	8.98	–	69.45
	CYP2A6	–	–	0.040	–	–	–	–
	CYP2B6	–	–	0.002	–	–	–	–
	CYP2C9	–	–	0.156	–	–	–	–
	CYP2C19	–	–	0.026	–	–	–	–

a) Metabolite formation rates were determined after 30 min incubation of 10 μM of each enantiomer together with 12.5 pmol enzyme.
b) Data according to [27].
c) Predicted metabolite formation rate in liver microsomes was calculated by multiplying the metabolite formation rate in SUPERSOMES by the relative contribution of an isoform to the total CYP content in liver microsomes.
d) Relative contribution of CYPs to PPF *N*-dealkylation was calculated to the percentage of the sum of predicted metabolite formation rates in liver microsomes.

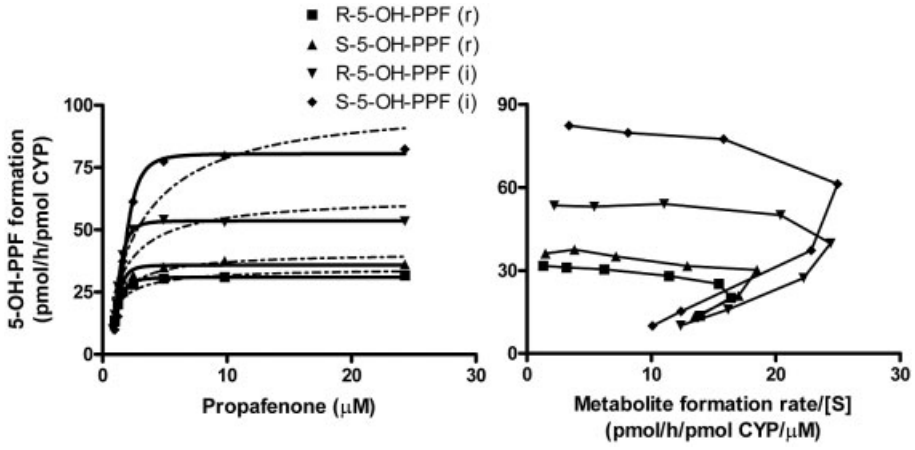

Figure 3. 5OH-PPF formation rate *versus* PPF enantiomer concentration (graphs of left panel) and Eadie–Hofstee plots (graphs of right panel) for the CYP2D6 *in vitro* metabolism of racemic, *R*- and *S*-PPF. Data in the left panel were fit to the Hill equation (autoactivation model, solid lines) and the Michaelis–Menten model (broken lines). Incubations with racemic and individual enantiomers are referred to as (r) and (i), respectively.

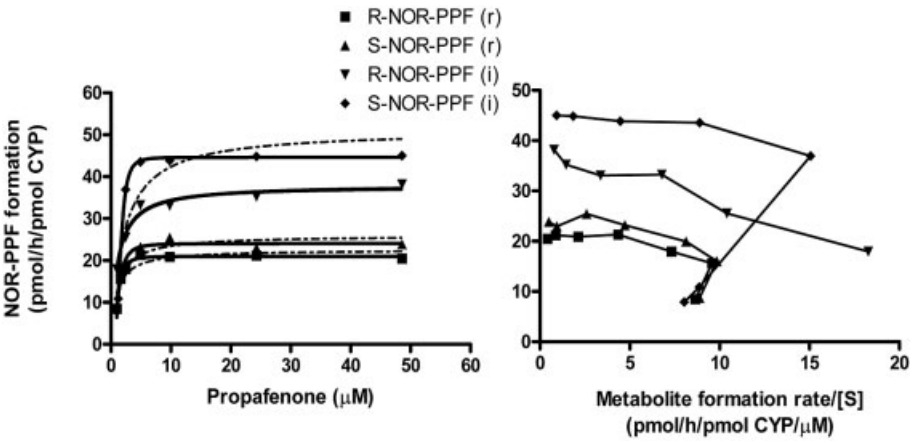

Figure 4. NOR-PPF formation rate *versus* PPF enantiomer concentration (graphs of left panel) and Eadie–Hofstee plots (graphs of right panel) for the CYP2D6 *in vitro* metabolism of racemic, *R*- and *S*-PPF. Data in the left panel were fit to the Hill equation (autoactivation model, solid lines) and the Michaelis–Menten model (broken lines). Incubations with racemic and individual enantiomers are referred to as (r) and (i), respectively.

and the corresponding CL_{int} and CL_{max} values calculated from Eqs. (4) and (5), respectively, are summarized in Table 2. The formations of *R*- and *S*-5OH-PPF obtained from racemic PPF and individual PPF enantiomers were found to follow atypical enzyme kinetics. The Hill equation (Eq. 2) provided the best fit to the experimental data (left-hand graph in Fig. 3), indicating that autoactivation takes place. Compared to the Michaelis–Menten model, the correlation coefficients (R^2) obtained for the autoactivation model were determined to be significantly higher (Table 2) and the *F*-test for the model comparison resulted in $p < 0.006$ (Table 2). The same was found to be true for the production of *R*- and *S*-NOR-PPF in presence of racemic PPF and *S*-PPF (left-hand graph in Fig. 4). Further analysis of the data resulted in hooked Eadie–Hofstee plots, suggesting autoactivation kinetics or allosterism (right-hand graphs in Figs. 3, 4). However, *R*-NOR-PPF formed from *R*-PPF followed Michaelis–Menten kinetics which is seen with the overlap of two regression lines in the left-hand graph of Fig. 4, the linear relationship in the right-hand graph of Fig. 4, the *n* value of the autoactivation model ($n = 1.04$) which is very close to unity, and the *F*-value of the model comparison ($p > 0.05$, Table 2).

When incubated separately, *S*-5OH-PPF was formed at a higher rate than *R*-5OH-PPF. V_{max} and K_m values of the *S*-PPF to *S*-5OH-PPF conversion were higher (1.5- and 1.43-fold, respectively) than those for the corresponding metabolism of *R*-PPF (Table 2). However, the CL_{max} values for both enantiomers were the same. The results obtained after incubation of the PPF racemate showed that the *S*-PPF to *S*-5OH-PPF transformation takes place at a slightly higher rate than the *R*-PPF to *R*-5OH-PPF hydroxylation. Incubation with individual *S*- and *R*-PPF enantiomers in comparison to racemic PPF revealed larger V_{max} values (2.25- and 1.73-fold, respectively), larger K_m values (1.56- and 1.17-fold, respectively), and larger CL_{max} values (1.42- and 1.55-fold, respectively).

For the incubation of the racemate, V_{max}, k', and CL_{max} values for the formation of both NOR-PPF enantiomers were found to be almost equal. V_{max} values of the metabolism of individual *S*- and *R*-PPF enantiomers were found to be higher than those of the incubation with the racemate. The same was observed for the CL_{max} values. V_{max} was found to be similar whereas clearance and K_m values were not equal when enantiomers were incubated individually. Clearance for the *R*-NOR-PPF formation was about twice that of the *S*-NOR-PPF production. The k' and K_m values for *R*-NOR-PPF formation were determined to be equal. However, this was not the case for *S*-NOR-PPF and the values were found to be higher than those of *R*-NOR-PPF formation.

3.3 Kinetics of CYP3A4 mediated *N*-dealkylation of PPF

The kinetics of PPF *N*-dealkylation in CYP3A4 microsomes incubated with racemic PPF (range: 5–250 μM of each enantiomer) together with corresponding nonlinear Eadie–Hofstee plots are shown in Fig. 5. Corresponding data obtained for incubations with individual PPF enantiomers (range: 5–1000 μM) are presented in Fig. 6. The estimates for two models, the single-site Michaelis–Menten and the substrate inhibition models, are summarized in Table 3. For the experiments with racemic PPF, it was interesting to find that the *N*-dealkylation activity decreased at enantiomer concentrations >50 μM (Fig. 5). The same was found to be true for concentrations above 100 μM in the case of incubations with the individual enantiomers (Fig. 6). A possible explanation for this phenomenon is substrate inhibition. Thus, not surprisingly, the fits obtained using Eq. (3) were found to describe the experimental behavior over the entire concentration range. This was not the case using the single-site Michaelis–Menten model (Figs. 5, 6, Table 3). How-

Table 2. Estimates of kinetic parameters and model comparison for the CYP2D6*1 data[a)]

Substrate	Product	Michaelis–Menten model				Autoactivation model					Model comparison (*F*-test)
		R^2	K_m	V_{max}	CL_{int}	R^2	k'	V_{max}	CL_{max}	n	*p*-value
Rac. PPF	*R*-5OH-PPF	0.8539	0.88 (0.24)	34.54 (2.29)	39.25	0.9913	1.04 (0.03)	31.00 (0.45)	15.88	3.09 (0.34)	0.0014
	S-5OH-PPF	0.8085	1.04 (0.36)	40.88 (3.64)	39.31	0.9769	1.12 (0.04)	35.85 (0.94)	17.89	3.73 (0.67)	0.0057
	R-NOR-PPF	0.8312	0.91 (0.29)	22.58 (1.40)	24.81	0.9893	1.13 (0.04)	21.00 (0.32)	9.57	2.64 (0.29)	0.0015
	S-NOR-PPF	0.8497	1.09 (0.34)	25.98 (1.71)	23.83	0.9820	1.24 (0.07)	24.06 (0.54)	9.85	2.42 (0.36)	0.0056
R-PPF	*R*-5OH-PPF	0.7921	1.54 (0.62)	63.25 (8.08)	41.07	0.9994	1.22 (0.01)	53.60 (0.24)	24.58	3.74 (0.10)	<0.0001
	R-NOR-PPF	0.9684	1.09 (0.16)	38.01 (1.03)	34.87	0.9686	1.09 (0.18)	37.75 (1.84)	29.42	1.04 (0.26)	0.8780
S-PPF	*S*-5OH-PPF	0.8355	2.87 (1.30)	101.50 (16.30)	35.36	0.9971	1.75 (0.04)	80.53 (1.26)	25.41	3.56 (0.26)	0.0001
	S-NOR-PPF	0.8144	2.06 (0.96)	51.08 (6.15)	24.79	0.9971	1.62 (0.05)	44.6 (0.57)	15.22	3.58 (0.26)	<0.0001

a) Units of measurements: K_m, μM; V_{max}, pmol·h^{-1} pmol^{-1} CYP; clearance, μL·h^{-1} pmol^{-1} CYP. Numbers in parentheses are standard errors.

Table 3. Estimates of kinetic parameters and model comparison for the CYP3A4 data[a)]

Substrate	Product	Michaelis–Menten model				Substrate inhibition model				Model comparison (*F*-test)
		R^2	K_m	V_{max}	CL_{int}	R^2	K_m	V_{max}	K_i	*p*-value
Rac. PPF	*R*-NOR-PPF	0.5529	4.64 (3.54)	36.32 (5.03)	7.82	0.9878	17.61 (3.25)	68.18 (6.56)	145.60 (30.53)	0.0019
	S-NOR-PPF	0.7074	6.31 (3.74)	29.60 (3.57)	4.69	0.9859	18.64 (3.84)	50.29 (5.23)	198.60 (49.67)	0.0046
R-PPF	*R*-NOR-PPF	0.6985	15.89 (10.24)	79.34 (10.53)	4.99	0.9890	73.76 (15.59)	176.6 (21.77)	397.60 (91.39)	< 0.0001
S-PPF	*S*-NOR-PPF	0.8671	14.71 (6.05)	96.76 (9.06)	6.58	0.9939	38.22 (5.87)	158.40 (12.47)	467.40 (91.06)	0.0008

a) Units of measurements: K_m, μM; V_{max}, pmol·h^{-1} pmol^{-1} CYP; clearance, μL·h^{-1} pmol^{-1} CYP. Numbers in parentheses are standard errors.

ever, for the kinetic analysis of the first part of the PPF dealkylation data, *i.e.*, the parts prior to the activity decreases, the data were found to fit well to the Michaelis–Menten model (Table 4).

For the truncated substrate concentration range, K_m values for the incubations with individual *R*- and *S*-PPF enantiomers were determined to be 55.08 ± 8.32 and 30.93 ± 2.71 μM, respectively, and corresponding values with racemic PPF were 11.68 ± 2.34 and 13.55 ± 3.71 μM, respectively. The V_{max} values were 140.7 ± 10.47 and 135.00 ± 4.91 pmol·h^{-1}pmol^{-1} CYP, respectively, for individual enantiomers and 51.78 ± 3.69 and 40.44 ± 4.24 pmol·h^{-1} pmol^{-1} CYP, respectively, for the incubation with the racemate. Corresponding clearance values were calculated to be 2.55, 4.36, 4.43, and

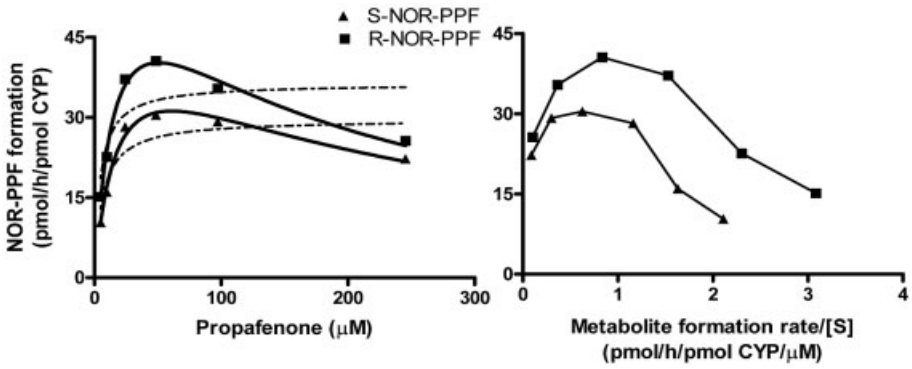

Figure 5. NOR-PPF formation rate *vs.* PPF enantiomer concentration (graphs of left panel) and Eadie–Hofstee plots (graphs of right panel) for the CYP3A4 *in vitro* metabolism of racemic PPF. Data in the left panel were fit to the substrate inhibition model (solid lines) and the Michaelis–Menten model (dashed lines).

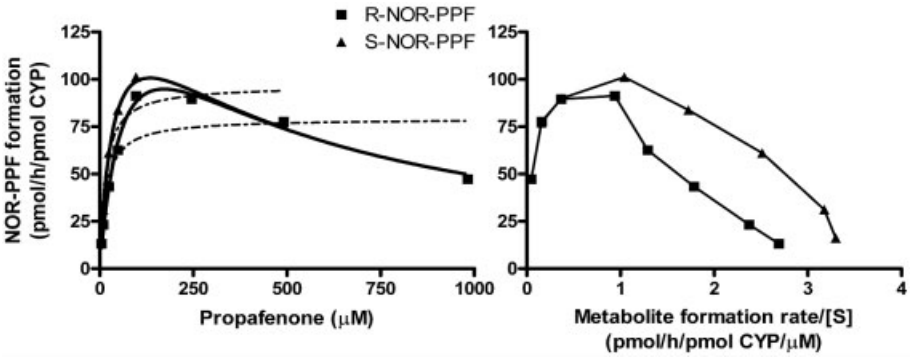

Figure 6. NOR-PPF formation rate *vs.* PPF enantiomer concentration (graphs of left panel) and Eadie–Hofstee plots (graphs of right panel) for the CYP3A4 *in vitro* metabolism of individual PPF enantiomers. Data in the left panel were fit to the substrate inhibition model (solid lines) and the Michaelis–Menten model (dashed lines).

Table 4. Estimates of kinetic parameters for truncated CYP3A4 data using the Michaelis–Menten model[a), b)]

Substrate	Product	Michaelis–Menten model			
		R^2	K_m	V_{max}	CL_{int}
Rac. PPF	*R*-NOR-PPF	0.9833	11.68 (2.34)	51.78 (3.69)	4.43
	S-NOR-PPF	0.9724	13.55 (3.71)	40.44 (4.24)	2.98
R-PPF	*R*-NOR-PPF	0.9949	55.08 (8.32)	140.7 (10.47)	2.55
S-PPF	*S*-NOR-PPF	0.9973	30.93 (2.71)	135.0 (4.91)	4.36

a) Data for 5–50 μM of the substrates (incubation with racemic PPF) and for 5–100 μM of the substrates (incubation with individual enantiomers).
b) Units of measurements: K_m, μM; V_{max}, pmol·h^{-1} pmol^{-1} CYP; clearance, μL·h^{-1} pmol^{-1} CYP. Numbers in parentheses are standard errors.

2.98 μL·h^{-1} pmol^{-1} CYP, respectively (Table 4). For the entire concentration range and using the substrate inhibition model (Eq. 2), K_m values were 73.76 ± 15.59, 38.22 ± 5.87, 17.61 ± 3.25, and 18.64 ± 3.84 μM, respectively, and V_{max} values were 176.6 ± 21.77, 158.40 ± 12.47, 68.18 ± 6.56, and 50.29 ± 5.23 pmol·h^{-1} pmol^{-1} CYP, respectively (Table 3). These data are quite similar to those obtained for the truncated substrate concentration range using the Michaelis–Menten model (Table 4). Application of the Michaelis–Menten model to all data revealed significantly lower values for K_m, V_{max}, and CL_{int} (Table 3).

4 Discussion

In this study, eight cDNA-expressed human CYP enzymes (SUPERSOMES) were screened for the first time to identify the enzymes involved in the PPF hydroxylation and *N*-dealkylation. Among these enzymes, only CYP2D6 produced 5OH-PPF suggesting that this pathway is selective. On the contrary, NOR-PPF was found to be formed *via* CYP1A1, CYP1A2, CYP3A4, and CYP2D6 pathways. Incubation of racemic PPF with CYP1A1 revealed an enantioselective formation of *R*- and *S*-NOR-PPF and a high-dealkylation activity. The latter aspect has

been reported previously by Botsch *et al.* [8] using yeast-infected cells expressing CYP1A1. However, CYP1A1 is expressed only after exposure to inducers (*e.g.*, smoking) and is hardly detected in the liver. Therefore, the extent to which it can affect the PPF metabolism is highly influenced by individual and environmental conditions. Furthermore, CYP3A4, CYP2D6, and CYP2A6 were also found to produce other PPF metabolites, metabolites for which we did not have any standards for identification [19]. As CYP3A4 is the most abundant cytochrome P450 in human liver [26, 27], the formation of such metabolites might play an important role in the metabolism of PPF, its pharmacokinetics, or even in its side effects.

In clinical situations, it has been shown that a plasma PPF concentration of higher than 1.5 μg/mL (4.39 μM) is necessary for the premature ventricular beats, couplet beats, and ventricular tachycardia beats to be suppressed by more than 90% [24]. As the drug concentrations around the enzymes in the liver are higher than the plasma concentrations, racemic PPF and individual PPF enantiomers at a concentration of 10 μM for each enantiomer were incubated for 30 min with each enzyme. As it is shown with the data presented in Table 1, the formation of NOR-PPF by the different enzymes is stereoselective and is reduced significantly when racemic PPF is incubated. This enantiomer–enantiomer interaction at the level of metabolism was reported previously *in vivo* [28, 29]. However, Botsch *et al.* [8] and Hemeryck *et al.* [14] showed that PPF *N*-dealkylation was not stereoselective *in vitro* using HLM. This discrepancy might be due to the fact that multiple active enzymes are present in the latter approach. Determining the contribution of each CYP isozyme at a clinically relevant substrate concentration is important to understand complex metabolic reactions. The contributions of specific CYP enzymes to the total metabolic clearance can be estimated from their relative abundance in the liver [27]. The results presented in this study according to CYP isoform abundance in the liver indicate that CYP3A4 provides the highest contribution to the NOR-PPF formation (Table 1). CYP1A2 also significantly contributes to *N*-dealkylation of PPF but its involvement is less than that of CYP3A4. These findings are in a good agreement with the results of Botsch *et al.* [8] who reported relative contributions for yeast-infected cells expressing CYP3A4 and CYP1A2 as being 75 and 22%, respectively. It is worth noting that the activity of CYP2D6 is higher than those of the other enzymes. However, considering its abundance in liver, it provides the least contribution to NOR-PPF formation.

For the last several years, a large number of examples of atypical enzyme kinetics have been observed in drug metabolism reactions [30–33]. The number of compounds exhibiting sigmoidal kinetics, however, has probably been underreported to date, owing to a lack of necessary analytical sensitivity required to characterize the initial portion of the velocity curve. In order to get the best estimate of kinetic parameters, it is necessary to apply an appropriate kinetic model to the *in vitro* data, especially when extrapolating the *in vitro* findings to the *in vivo* conditions. Two kinds of atypical kinetic models (autoactivation and substrate inhibition) were found to provide a proper explanation of the PPF metabolism in the presence of CYP2D6 and CYP3A4 SUPERSOMES. With the exception of the dealkylation in presence of *R*-PPF, all CYP2D6-induced kinetics were found to follow the Hill equation (autoactivation kinetics, Table 2). For these systems, clearance is dependent on substrate concentration. Using the Michaelis–Menten model, an overestimation of the clearance would be obtained. It has been hypothesized that most atypical enzyme kinetics are caused by the simultaneous binding of more than one substrate molecule to the active sites of an enzyme. Therefore, the metabolism of substrates may occur from either binding site or the presence of a second substrate molecule binding within the active site produces some kind of change in enzyme efficiency, including reduced uncoupling and conformational change [21], processes which might be stereoselective. In our study, artifactual sources, including protein overload and high substrate consumption [22], can be excluded. However, lack of analytical sensitivity might have hindered the determination of the initial portion of the curve ($<$0.8 μM enantiomer concentration). To the best of our knowledge, this is the first example of a sigmoidal kinetics by the CYP2D6 enzyme. Furthermore, it is the first investigation of the PPF kinetics in presence of CYP2D6 only. Interestingly, *R*-NOR-PPF formation in the 0.8–50 μM incubation with individual *R*-PPF was best fitted with the single-site Michaelis–Menten model. Its interaction with the enzyme appears to be different than that of *S*-PPF.

For CYP3A4, the kinetics of *R*- and *S*-NOR-PPF formation can be very well described by the substrate inhibition model. Ignoring any evidence of convexity in the rate *versus* substrate concentration profile results in an underestimation of K_m and V_{max} and overestimation of clearance (Michaelis–Menten data, Tables 3, 4). In the case of substrate inhibition, clearance initially follows the Michaelis–Menten case but decreases more rapidly in the saturation portion of the curve due to the impact of the inhibition effect [22]. In clinical use, the concentration of PPF is unlikely to reach 50 μM. Thus, the initial part of the data which could be well fitted to the Michaelis–Menten model were used to calculate clearance (Table 4). It has been shown that substrate depletion due to metabolism may produce an apparent atypical kinetics [21]. In our

work, we showed that CYP3A4 produces more than one metabolite (Fig. 2 and [19]). With an increase of the substrate concentration, the peak magnitudes of the unknown metabolites decreased as well, indicating that inhibition is also taking place for the formation of these compounds. As substrate depletion was controlled to be less than 15%, production of these metabolites is unlikely to be a source of artifacts. Furthermore, no solubility problems were noted. Thus, substrate inhibition may indeed be responsible for the observed atypical kinetics. However, Zhou *et al.* did not report any atypical kinetics evaluating metabolism of PPF by liver CYP3A4 expressed in transgenic Chinese hamster CHL cell lines [17]. It must be noted that the catalytic activity of CYP3A4 can be influenced by various incubation conditions. The atypical kinetics of CYP3A4 mediated PPF dealkylation were determined in the presence of cytochrome b_5 and magnesium, compounds that have been shown to influence the CYP3A4 activity [34]. Maenpaa *et al.* [35] reported that the buffer composition, ionic strength, and the source of assay constituents affected the midazolam hydroxylation activity. Furthermore, the kinetics of the oxidation of pyrene by CYP3A4 was found to be sigmoidal in the absence of magnesium but biphasic in the presence of magnesium [36]. For the assessment of these parameters on the CYP3A4 PPF metabolism, further investigations under different incubation conditions will have to be conducted.

For the comparison of the PPF metabolite formation kinetics in presence of CYP2D6 and CYP3A4, individual enantiomers and the racemate were incubated separately. For the hydroxylation with CYP2D6, as is shown in Table 2, the V_{max} and k' values for both metabolites of *S*-PPF are higher than those obtained with *R*-PPF. Moreover, both V_{max} and k' decreased when the racemate was used as substrate. The results obtained in this study are in good agreement with those of Kroemer *et al.* [13] who evaluated the PPF 5-hydroxylation in HLM. Despite the difference in k' and V_{max}, clearance of the two enantiomers was estimated to be nonstereoselective in incubations with individual enantiomers and with racemic PPF. *In vivo*, it has been reported that *R*-PPF shows a higher clearance than its antipode in both extensive and poor metabolizers of debrisoquine, with the degree of stereoselectivity being almost the same in both populations [37]. Kroemer *et al.* [13] and Hemeryk *et al.* [14] also showed that the intrinsic clearances of the enantiomers of PPF for the hydroxylation pathway are very similar after the incubation of all substrates with HLM. As we showed in this study, CYP2D6 is selective for 5OH-PPF formation which can explain the similarity observed in calculation of clearance in CYP2D6 SUPERSOMES, HLM, and *in vivo*. Therefore, it appears that CYP2D6 is not responsible for the stereoselective clearance of PPF.

The K_m values obtained for the CYP2D6 formation of NOR-PPF are rather low. Low values were previously reported for the CYP2D6-mediated *O*-demethylation of dextromethorphan [38] and are a characteristic for low-capacity, high-affinity enzymes. On the other hand, K_m values for CYP3A4 transformations were noted to be much larger. For CYP3A4 and incubation with individual enantiomers, the K_m value obtained for *R*-PPF was significantly higher than that of *S*-PPF. On the contrary to K_m, a slight difference was observed between the V_{max} and K_i values. Furthermore, all kinetic parameters were significantly decreased in the case of the incubation with racemic PPF. When individual enantiomers were incubated, the clearance for *S*-PPF appeared to be higher than that of *R*-PPF. The opposite results were observed for racemic PPF. These data are in good agreement with those of *in vivo* studies in which individual enantiomers and racemic PPF were administered [5]. Therefore, CYP3A4 appears to be one of the enzymes responsible for the stereoselective metabolism of PPF.

In summary, this paper reports the first investigation of the PPF hydroxylation and dealkylation kinetics by the CYP2D6 enzyme. CYP2D6 provides a minor contribution to *N*-dealkylation of PPF. Except for the dealkylation of individually incubated *R*-PPF, the kinetic profiles obtained for CYP2D6 are best described by sigmoidal kinetics. An overestimation of the clearance would be obtained if a hyperbolic curve would be forced through the data to obtain the kinetic parameters. The nonstereoselective clearance values obtained for the CYP2D6 hydroxylation are in good agreement with those of HLM and *in vivo* studies. CYP3A4 exhibits the highest contribution to the PPF metabolism. PPF *N*-dealkylation profiles best fit to the substrate inhibition model. Clearance values obtained with CYP3A4 are stereoselective and are consistent with the *in vivo* results. This is the first paper reporting enantioselective CE data that led to the elucidation of the kinetics of metabolic steps of a drug in presence of single enzymes. The sensitive CE method applied in this study allowed a more detailed analysis of PPF sigmoidal kinetics by CYP2D6. Moreover, the possibility to simultaneously quantify the enantiomers of NOR-PPF and 5OH-PPF permitted the investigation of the enantioselective PPF *N*-dealkylation and hydroxylation kinetic profiles using the metabolite formation approach.

The authors would like to thank Dr. Ute Hofmann for the standard compounds of 5OH-PPF and NOR-PPF and Dr. Markus Wenk, Department of Clinical Pharmacology, University of Basel, Switzerland, for the loan of the BioFocus 3000. This work was partly sponsored by the Swiss National Science Foundation.

5 References

[1] Atkins, W. M., *Drug Discov. Today* 2004, *9*, 478–484.

[2] Wilkinson, G. R., *New Engl. J. Med.* 2005, *352*, 2211–2221.

[3] Harron, D. W. G., Brogden, R. N., *Drugs* 1987, *34*, 617–647.

[4] Dollery, C., *Therapeutic Drugs*, 2nd Edn., Churchill Livingstone, Edinburgh, UK 1999, p243–p248.

[5] Mehvar, R., Brocks, D. R., Vakily, M., *Clin. Pharmacokinet.* 2002, *41*, 533–558.

[6] Hii, J. T. Y., Duff, H. J., Burgess, E. D., *Clin. Pharmacokinet.* 1991, *21*, 1–10.

[7] Kroemer, H. K., Mikus, G., Kronbach, T., Meyer, U. A., Eichelbaum, M., *Clin. Pharmacol. Ther.* 1989, *45*, 28–33.

[8] Botsch, S., Gautier, J.-C., Beaune, P., Eichelbaum, M., Kroemer, H. K., *Mol. Pharmacol.* 1993, *43*, 120–126.

[9] Brandon, E. F., Raap, C. D., Meijerman, I., Beijnen, J. H., Schellens, J. H., *Toxicol. Appl. Pharmacol.* 2003, *189*, 233–246.

[10] Tan, W., Li, Q., McKay, G., Semple, H. A., *J. Pharm. Biomed. Anal.* 1998, *16*, 991–1003.

[11] Morita, K., Mizuochi, M., Yamaji, A., Yokoyama, T., *Biol. Pharm. Bull.* 1994, *17*, 531–534.

[12] Anzenbacherova, E., Anzenbacher, P., Svoboda, Z., Ulrichova, J. *et al.*, *Biomed. Papers* 2003, *147*, 155–159.

[13] Kroemer, H. K., Fischer, C., Messe, C. O., Eichelbaum, M., *Mol. Pharmacol.* 1991, *40*, 135–142.

[14] Hemeryck, A., De Vriendt, C., Belpaire, F. M., *J. Clin. Psychopharmacol.* 2000, *20*, 428–434.

[15] Kroemer, H. K., Botsch, S., Heinkele, G., Schick, M., *Methods. Enzymol.* 1996, *272*, 99–105.

[16] Reder-Hilz, B., Ullrich, M., Ringel, M., Hewitt, N. *et al.*, *Naunyn-Schmiedeberg's Arch. Pharmacol.* 2004, *369*, 408–417.

[17] Zhou, Q., Yao, T.-W., Yu, Y.-N., Zeng, S., *Acta Pharmacol. Sin.* 2001, *22*, 944–948.

[18] Zhou, Q., Yao, T.-W., Yu, Y.-N., Zeng, S., *Pharmazie* 2003, *58*, 651–653.

[19] Afshar, M., Thormann, W., *Electrophoresis*, 2006, *27*, 1517–1525.

[20] Tracy, T. S., Hummel, M. A., *Drug Metab. Rev.* 2004, *36*, 231–242.

[21] Tracy, T. S., *Curr. Drug Metab.* 2003, *4*, 341–346.

[22] Houston, B. J., Kenworthy, K. E., *Drug Metab. Dispos.* 2000, *28*, 246–254.

[23] Houston, B. J., Galetin, A., *Arch. Biochem. Biophys.* 2005, *433*, 351–360.

[24] Zoble, R. G, Kirsten, E. B., Brewington, J., *Clin. Pharmacol. Ther.* 1989, *45*, 535–541.

[25] Keller, K., Meyer-Estorf, G., Beck, O. A., Hochrein, H., *Eur. J. Clin. Pharmacol.* 1978, *13*, 17–20.

[26] Shimada, T., Yamazaki, H., Mimura, M., Inui, Y., Guengerich, F. P., *J. Pharmacol. Exp. Ther.* 1994, *270*, 414–423.

[27] Wojcikowski, J., Pichard-Garcia, L., Maurel, P., Daniel, W. A., *Eur. Neuropsychopharmacol.* 2004, *14*, 199–208.

[28] Li, G., Gong, P.-L., Qiu, J., Zeng, F.-D., Klotz, U., *Br. J. Clin. Pharmacol.* 1998, *46*, 441–445.

[29] Kroemer, K., Fromm, M. F., Bühl, K., Terefe, H. *et al.*, *Circulation* 1994, *89*, 2396–2400.

[30] Lin, Y., Lu, P., Tang, C., Mei, Q. *et al.*, *Drug Metab. Dispos.* 2001, *29*, 368–374.

[31] Stone, A. N., Mackenzie, P. I., Galentin, A., Houston, J. B., Miners, J. O., *Drug Metab. Dispos.* 2003, *31*, 1086–1089.

[32] Korzekwa, K. R., Krishnamachary, N., Shou, M., Ogai, A. *et al.*, *Biochemistry* 1998, *37*, 4137–4147.

[33] Tracy, T.S., Hutzler, J. M., Haining, R. L., Rettie, A. E. *et al.*, *Drug Metab. Dispos.* 2002, *30*, 385–390.

[34] Hutzler, J. M., Tracy, T. S., *Drug Metab. Dispos.* 2002, *30*, 355–362.

[35] Maenpaa, J., Hall, S. D., Ring, B. J., Strom, S. C., Wrighton, S. A., *Pharmacogenetics* 1998, *8*, 137–155.

[36] Schrag, M. L., Wienkers, L. C., *Drug Metab. Dispos.* 2000, *28*, 1198–1201.

[37] Kroemer, H. K., Funck-Brentano, C., Silberstein, D. J., Wood, A. J. J. *et al.*, *Circulation* 1989, *79*, 1068–1076.

[38] Von Moltke, L. L., Greenblatt, D. J., Grassi, J. M., Granda, B. W. *et al.*, *J. Pharm. Pharmacol.* 1998, *50*, 997–1004.

